CrossMark
click for updates

View Article Online
View Journal

Journal of Materials Chemistry C

Accepted Manuscript

This article can be cited before page numbers have been issued, to do this please use: A. Castro, J. Morère, A. CABAÑAS, L. Ferreira, M. Godinho, P. Ferreira and P. M. Vilarinho, *J. Mater. Chem. C*, 2016, DOI: 10.1039/C6TC04232E.

This is an Accepted Manuscript, which has been through the Royal Society of Chemistry peer review process and has been accepted for publication.

Accepted Manuscripts are published online shortly after acceptance, before technical editing, formatting and proof reading. Using this free service, authors can make their results available to the community, in citable form, before we publish the edited article. We will replace this Accepted Manuscript with the edited and formatted Advance Article as soon as it is available.

You can find more information about Accepted Manuscripts in the author guidelines.

Please note that technical editing may introduce minor changes to the text and/or graphics, which may alter content. The journal's standard Terms & Conditions and the ethical guidelines, outlined in our author and reviewer resource centre, still apply. In no event shall the Royal Society of Chemistry be held responsible for any errors or omissions in this Accepted Manuscript or any consequences arising from the use of any information it contains.

ROYAL SOCIETY OF CHEMISTRY

rsc.li/materials-c

View Article Online
DOI: 10.1039/C6TC04232E

Published on 19 December 2016. Downloaded by University of Massachusetts - Amherst on 09/01/2017 14:51:29.

Designing nanocomposites using supercritical CO_2 to insert Ni nanoparticles into the pores of nanopatterned $BaTiO_3$ thin films

Alichandra Castro[1], Jacobo Morère[2], Albertina Cabañas[2], Liliana P. Ferreira[3,4], Margarida Godinho[3], Paula Ferreira[1*], Paula M. Vilarinho[1*]

[1] CICECO – Aveiro Institute of Materials, Department of Materials and Ceramic Engineering, CICECO, University of Aveiro, 3810-193 Aveiro, Portugal

[2]Departamento de Química-Física I, Universidad Complutense de Madrid, 28040 Madrid, Spain

[3]Biosystems and Integrative Sciences Institute (BioISI), Faculdade de Ciências, Universidade de Lisboa, 1749-016 Lisboa, Portugal

[4]Department of Physics, University of Coimbra, 3004-516 Coimbra, Portugal

Abstract

A new concept to prepare nanocomposite thin films is explored. Two chemical-based bottom-up steps are used to design functional films including: i) block copolymer-assisted self-assembly of a porous matrix; and ii) impregnation of nanoparticles from a ferroic phase within the pores by supercritical CO_2 deposition. Porous nanopatterned $BaTiO_3$ thin films with *ca*. 17 nm of thickness are prepared using a cost-effective sol-gel solution containing a block copolymer and evaporation-induced self-assembly methodology. Hexagonal-arranged pores with diameter of *ca.* 95 nm, running perpendicularly to the substrate are filled with Ni nanoparticles using the supercritical fluid deposition technique from reduction of hydrated nickel nitrate in a supercritical CO_2-ethanol mixture at 250 ºC. Small Ni nanoparticles with 21 ± 5 nm nm are

Journal of Materials Chemistry C Accepted Manuscript

View Article Online
DOI: 10.1039/C6TC04232E

Published on 19 December 2016. Downloaded by University of Massachusetts - Amherst on 09/01/2017 14:51:29.

selectively deposited inside the pores of the porous matrix. Structural and magnetic properties prove the coexistence of both phases.

Keywords

Nanocomposite thin films; nanopatterned porous films, supercritical CO_2 deposition, Ni nanoparticles, functional

Introduction

Porous films may be seen as "bottom-up" platforms for nanotechnology.[1–3] Oxide-based porous films can find important applications at the microelectronics and photonics fields not only by nanofabricating functional ordered porous patterns with lateral thickness below 100 nm,[4,5] but also by finding strategies to insert functional molecules or nanoparticles inside of the pores.[1]

We have recently prepared and characterized the structure of nanoporous and nanopatterned thin films with $PbTiO_3$ composition by evaporation-induced self-assembly (EISA).[6,7] Over the last decade, EISA has been exploited for the preparation of mesoporous metal oxide thin films with periodicities in the sub-50 nm size range.[2] Besides the synthesis and structural characterization, we also demonstrated the positive effect of porosity on local ferroelectric properties of $PbTiO_3$.[6,7] Well-ordered porous structures are excellent matrices to create multifunctional materials. We wish now to exploit the potential of these porous platforms, with vertical aligned pores perpendicularly to the substrate, by depositing a magnetic material inside the pores of the ferroelectric patterned films. The vertical architectures of the composites should lead to enhanced properties compared to the layered structure as consequence of the increase

Journal of Materials Chemistry C Accepted Manuscript

View Article Online
DOI: 10.1039/C6TC04232E

Published on 19 December 2016. Downloaded by University of Massachusetts - Amherst on 09/01/2017 14:51:29.

of interfacial area between the two ferroic phases and of the reduction substrate clamping effect.[8]

The deposition of the second magnetic phase within the small pores of a porous multimetallic oxide matrix is quite challenging because of the difficulties in filling the pores without covering the all surface and achieving good interfaces between both crystallographic phases. In order to overcome these limitations, we proposed to use supercritical CO_2 as a solvent.

The use of supercritical fluids (SCFs) in Materials Science started in the beginning of the 90s as a mean to produce nanomaterials.[9–12] Among all nanomaterials, the nanoparticles and nanostructured materials are the most explored areas.[10] The interest in using SCFs relies on their unique properties, high solvating power and excellent transport properties. Indeed, within the supercritical region, there is no phase boundary between the gas and liquid phases, meaning that there is a continuity in the physical properties of the fluid between the gas and liquid states.[9]

The most frequently used supercritical fluid is carbon dioxide (CO_2). CO_2 is cheap, non-flammable, chemically inert, not toxic and has a relatively low critical temperature and pressure (T_C = 31 ºC, P_C = 7.38 MPa).[13] Supercritical CO_2 can dissolve a broad range of organometallic compounds.[14–16] Although pure CO_2 is not a good solvent for inorganic metal salts, however hydrated metal nitrates and chlorides can be dissolved in supercritical CO_2 by adding a small amount of a polar solvent such as ethanol in CO_2-ethanol solutions.[17] These precursors are less toxic, cheaper and easier to handle than the nickel organometallic compounds.

Watkins *et al.* developed a SCF based approach that consists in the deposition of metals and metal oxide by chemical reaction of suitable precursors in an SCF within a high-pressure reactor.[16,20] The reaction was generally initiated upon the addition of hydrogen

Journal of Materials Chemistry C Accepted Manuscript

View Article Online
DOI: 10.1039/C6TC04232E

Published on 19 December 2016. Downloaded by University of Massachusetts - Amherst on 09/01/2017 14:51:29.

(H_2) or another reducing agent such as an alcohol. The Supercritical Fluid Deposition Technique (SCFD) was used previously to deposit Ni films onto planar and patterned silicon wafers using supercritical CO_2 ($scCO_2$) [21,22] to achieve conformal films with high quality. The same approach was extended to deposit Ni nanoparticles into porous supports.[22–26] The low surface tension, high diffusivity and low viscosities of CO_2 solutions allow to deposit or incorporate metallic nanoparticles into a wide variety of inorganic and organic substrates for microelectronic, optical and catalytic applications. Although the SCFD is a solution based approach, the transport properties of SCFs, which are more like to those of a gas, afford the infiltration in the complex geometry and avoid the mass transfer limitations common to liquid phase reductions. The high solubility of the decomposition products in CO_2 enhances purity of the material deposited at low temperature by facilitating desorption of potential contaminants from its surface.[5] Furthermore, the metal loading is easy to control by adjusting concentration, deposition time and pressure.

To the best of our knowledge, SCFD has never been used to prepare nanocomposite thin films. In this paper, the preparation of the nanopatterned $BaTiO_3$ thin films by EISA onto platinized silicon wafer, the deposition of Ni within the pores using SCFD, and the structural and physical characterization of the materials are described. We prove a new concept for nanocomposite preparation using a full chemical scalable approach. This approach may be interesting for the design of multiferroic nanocomposite films, i.e. films exhibiting both magnetic spin and electric dipole ordering, in a vertical heterogeneous (1-3) arrangement as represented in Scheme 1. Multiferroics are very promising materials for modern electronics especially high density magnetic storage, sensors, and spintronics.[27] Furthermore, single-phase multiferroics are scarce and

Journal of Materials Chemistry C Accepted Manuscript

View Article Online
DOI: 10.1039/C6TC04232E

Published on 19 December 2016. Downloaded by University of Massachusetts - Amherst on 09/01/2017 14:51:29.

composite multiferroic thin films must be designed in a way that enhances cross-coupling properties that enable applications.[28–30]

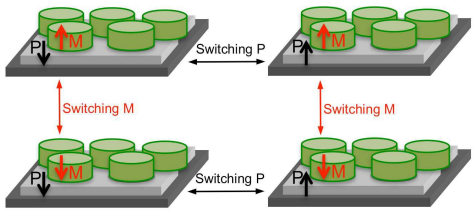

Scheme 1. Representation of the potential multiferroic application of the developed nanocomposite thin films.

Experimental

- **Nanopatterned thin films preparation**

Nanopatterned $BaTiO_3$ thin films were prepared using an adapted sol-gel method and evaporation induced self-assembly methodology as described in reference [7]. Poly(butadiene(1,4 addition)-b-ethylene oxide) (PB51-*b*-PEO62) amphiphilic block-copolymer, with MW_{PB} = 51 000 $gmol^{-1}$ and MW_{PEO} = 62 000 $gmol^{-1}$, was used as a structure-directing agent. Three solutions were prepared. In solution A, PB51-*b*-PEO62 block-copolymer (30 mg, Polymer Source) was dissolved in a mixture of absolute ethanol (119.86 mmol, Riedel-de Haën) at 70 ºC. Solution B was prepared by the dissolution of barium hydroxide octahydrate (0.20 mmol, Merck, purity ≥ 98.0% w/w) in glacial acetic acid (8.93 mmol, Merck) at room temperature. Solution C was prepared from mixing 2,4-pentanedione (0.11 mmol, Fluka, purity 99.3% w/w) with titanium (IV) *n*-butoxide (0.20 mmol, Merck, 98.0% w/w) under stirring at room temperature. Afterwards, solutions B and C were added to solution A, forming the final solution. Nanopatterned $BaTiO_3$ thin films were deposited by dip-coating onto platinized silicon ($Pt/TiO_2/SiO_2/Si$) (Radiant Inc.) at 1.6 mm/s. All films were thermally treated in air at

Journal of Materials Chemistry C Accepted Manuscript

View Article Online
DOI: 10.1039/C6TC04232E

Published on 19 December 2016. Downloaded by University of Massachusetts - Amherst on 09/01/2017 14:51:29.

350 ºC during 5 min in order to complete the inorganic condensation (mesostructuration) of the matrix and to partially decompose the organic content. The films were also thermal treated at 600 and 700 ºC during 2 min.

- **Functionalization using a $scCO_2$**

The experiments were conducted in a *ca*. 100 mL stirred high-pressure reactor (Autoclave Eng. Inc.) in the batch mode. Several pieces of 1 cm x 1 cm of the nanopatterned $BaTiO_3$ thin films were placed vertically inside the high-pressure reactor and in contact with the wall. The nickel (II) nitrate hexahydrate precursor, (0.069 mmol, Sigma-Aldrich, 98.5% w/w) was previously dissolved in ethanol (68.50 mmol, Carlos ERBA) and placed in a vial allocated at the bottom of the reactor without contacting the substrates.

The reactor was then heated by a heating jacket connected to a PDI controller to 60 ºC and then filled with CO_2 (Air Liquid, purity >99.99 %) using a high-pressure syringe pump (Isco, Inc. Model 260D) thermostated at the same temperature up to 10.0 MPa. The temperature was measured using a K-type thermocouple. The pressure was measured using a pressure gauge. The mixture of the inorganic precursor with ethanol and $scCO_2$ was kept at these conditions for 1 h. The percentage of ethanol in CO_2 in the mixture was 9.5% mol. Then the reactor was heated at 250 ºC for 2 h. The precursor dissolved in $scCO_2$ impregnated the nanopatterned material and during heating decomposed. During these experiments the pressure was kept below 30.0 MPa (which is the maximum pressure of the equipment) by venting a small amount of the CO_2 solution from 100 ºC. Then, the heater was turned off and the reactor was depressurized through a needle valve in 1 h. Ethanol acted as co-solvent favouring precursor dissolution and as reducing agent at high temperature promoting chemical reduction of the salt.

- **Characterization**

Journal of Materials Chemistry C Accepted Manuscript

View Article Online
DOI: 10.1039/C6TC04232E

Published on 19 December 2016. Downloaded by University of Massachusetts - Amherst on 09/01/2017 14:51:29.

The film microstructure was investigated by high-resolution SEM using a SU-70 Hitachi microscope. The average pore and nanoparticle sizes were determined using the using the software Image J (version 1.45s).[31] The values presented are average values taken from the measurement of at least fifty different particles. The Atomic Force Microscopy (AFM) and Magnetic Force Microscopy (MFM) measurements were carried out on Nanoscope III, using Tap300 cantilevers with Al-coated tips (Budget Sensors, resonant frequency of 200−400 kHz, force constant of 20−75 N/m) and MESP cantilevers with CoCr-coated tips (Bruker, resonant frequency of 75−100 kHz, force constant of 2.8−5.0 N/m), respectively. The AFM images were collected in contact mode. In the MFM measurements, the topography signals of the film surface were taken simultaneously with the deflection and phase signals and were collected in non-contact mode. Since the results were obtained with the same type of cantilevers and under identical scanning and acquisition conditions, comparison between both films can be made. Magnetization measurements as a function of temperature and applied magnetic field were performed using a SQUID magnetometer (QD-MPMS). The thermal variation was measured at 200 Oe, increasing the temperature from 10 to 370 K after cooling the sample down to 10 K in zero applied field (zero field cooled - ZFC) or under the measurement field (field cooled - FC). The isothermal hysteresis loops were obtained at 35 K and 300 K for magnetic fields up to 5.5 T, parallel and perpendicular to the film surface. The diamagnetic components due to the substrate and to the porous $BaTiO_3$ film were subtracted from the measured magnetic moment.

Results and discussion

The pores of $BaTiO_3$ nanopatterned porous thin films were filled with Ni nanoparticles using supercritical CO_2 deposition method. Figure 1 shows top view SEM micrographs

Journal of Materials Chemistry C Accepted Manuscript

View Article Online
DOI: 10.1039/C6TC04232E

Published on 19 December 2016. Downloaded by University of Massachusetts - Amherst on 09/01/2017 14:51:29.

of nanopatterned $BaTiO_3$ thin films before (a-c) and after (e-g) functionalization with Ni and thermally treated at different temperatures. These micrographs are representative of the entire covered surfaces and exhibit the good quality of the hexagonal ordered porous structures. This pore order and periodicity result from the self-assembly of micelles of the amphiphilic block-copolymer, followed by condensation of the inorganic species around the micelle arrays. Figures 1a reveals an amorphous character of the structure after thermal treatment at 350 °C for 5 min. At this temperature all pores are already open due to the complete decomposition of the block copolymer and to the very thin deposited layer of the nanopatterned $BaTiO_3$ films. During the thermal decomposition of the block-copolymer, void motifs are thus created. The Pt grain structure of the $Pt/TiO_2/SiO_2/Si$ substrate can be already observed and demonstrates that vertical pores are open. Upon thermal treatment at 600 °C, the well-ordered porous structure remained without coalescence of the pores as seen in Figure 1b. However, at 700 ºC some walls between the pores start to collapse and the coalescence of some pores takes place (Figure 1c). Despite that, at this temperature the well-ordered array is practically kept at large scale. XRD measurement (not shown) did not confirm the crystallinity of the $BaTiO_3$ film treated at 700 °C. Potential explanations for the absence of XRD signals may be: i) the non-formation of the ferroelectric crystalline phase due to inadequate inorganic/organic ratio[32–35] or crystallization temperature; or ii) the crystallites or the coherent volume are too small to be detected by the XRD diffractometer. It has been reported the preparation by molecular beam epitaxy of crystalline $BaTiO_3$ thin films with thickness below 2 nm.[36] In our case the chemical-based preparation methodology and the low processing temperature would not only lead to polycrystalline structure but also would favor an incipient crystallization. Moreover, it is unknown the combined effect of the thickness (~17 nm) with the porosity on the ferroelectric properties.

Journal of Materials Chemistry C Accepted Manuscript

View Article Online
DOI: 10.1039/C6TC04232E

Published on 19 December 2016. Downloaded by University of Massachusetts - Amherst on 09/01/2017 14:51:29.

The analysis of the nanoscale ferroelectric properties was dismissed in consequence of the lack of evidence of crystalline structure. Despite the unclear crystallographic structure of the nanopatterned $BaTiO_3$ thin film thermal treated at 600 ºC, the prepared nanopatterned thin films were used as matrices for studying the functionalization with Ni nanoparticles through the SCFD approach (Figure 1d) to prepare a multifunctional material (Figure 1e-f). Basically, the SCFD approach involved the dissolution of the $Ni(NO_3)_2$ salt in the CO_2-EtOH mixture and the exposure of the substrate to the solution. After incorporation of the precursor on the substrate surface, the metallic precursor was reduced to its metal form by heating at 250 ºC. In this case, ethanol acted as both co-solvent and reducing agent. Thus, from the SEM micrographs, Figure 1e-f, no solvent residue or big nanoparticle clusters on the surface of the nanopatterned thin films were found. The presence of distinct nanoparticles only within the pores and more than one in the same pore can be also observed, suggesting that the particles coalescence was limited by the relatively low reduction temperature (Figure 1e-f). The nanoparticles are only placed inside the pores as an effect of the grained structure of the exposed platinum substrate which may catalyze the reduction.[37] Furthermore, Kondoh [38] reported the selective deposition on metal surfaces. The author demonstrated that Ru films, deposited in $scCO_2$ fluid, grew only on conductive or metallized surfaces due to their ability to donate electrons, attracting the chemical species to adsorb. So, similarly Ni nanoparticles are deposited within the vertical pores of the $BaTiO_3$ film on the top of the platinum substrate, which attracts the nickel precursor and helps on its reduction.

The average pore diameter and nanoparticles sizes determined from the SEM micrograph analysis are 95 ± 11 nm and 21 ± 5 nm, respectively. The nanoparticles seem from Figure 1e-f to very uniforms. The chemical composition of the nanoparticles was evaluated by EDX, confirming that nanoparticles are composed of Ni (Figure 1h).

Journal of Materials Chemistry C Accepted Manuscript

View Article Online
DOI: 10.1039/C6TC04232E

Published on 19 December 2016. Downloaded by University of Massachusetts - Amherst on 09/01/2017 14:51:29.

Figure 2 shows the AFM measurements performed in the nanopatterned $BaTiO_3$ thin films thermally treated at 600 ºC before (a) and after (b) functionalization with Ni. As like SEM micrographs the images are representative of the entire covered surfaces and exhibit good quality arrays of hexagonally-like ordered porous structure (Figure 2a). Figure 2b shows that more than 70 % of the pores of nanopatterned thin film are occupied by nanoparticles with *ca*. 21 nm in diameter. Several nanoparticles have been deposited per pore, suggesting that the functionalization was successful in addressing the nanoparticles into the pores only. The pore size is in good agreement with that measured in the SEM micrographs. The wall thickness between the pores is 43± 10 nm showing the small importance of the wall area compared to the pore size (69 ± 2 % porosity). As the AFM measurements were performed in contact mode with high resolution tips with tip height of 17 μm and tip radius < 10 nm, the depth pore can be related with film thickness. Thus, the thickness of the nanopatterned $BaTiO_3$ thin films is around 17 ± 2 nm. From the acquisition conditions and the relation between the depth pore and thickness it is possible to observe that the pores reach down to the substrate and the porosity is completely open and directed to the substrate as it was observed in the SEM micrographs. The RMS (root mean square) surface roughness for the nanopatterned thin films (Figure 2a) is 5.1 nm. However, the AFM images for Ni functionalized nanopatterned $BaTiO_3$ thin films (Figure 2b), present a RMS surface roughness of 3.0 nm. The decrease of the surface roughness proves that the pores are filled with nanoparticles, with consequent flattening of the surface. As for crystalline $BaTiO_3$, the Ni nanoparticles could not be identified by XRD. Again, due to the low film thickness, the Ni content may be below the resolution limit of the equipment.

In order to evaluate the magnetic behavior, the MFM measurements were performed in the Ni functionalized nanopatterned $BaTiO_3$ thin films (Figure 3). The topography and

Journal of Materials Chemistry C Accepted Manuscript

View Article Online
DOI: 10.1039/C6TC04232E

Published on 19 December 2016. Downloaded by University of Massachusetts - Amherst on 09/01/2017 14:51:29.

phase are shown in Figure 3a and 3b, respectively. The topography is very similar to the one obtained in SEM micrographs (Figure 1) and by AFM (Figure 2) showing the well-ordered porous structure filled with Ni nanoparticles. However, no contrast coming from the magnetic nanoparticles can be observed in the phase image even at 5 nm from the surface (Figure 3b) suggesting that the domains are oriented parallel to the surface and cannot be detected by our system that only operates in out of plane.

Figure 4 presents the magnetization measurements as a function of temperature and applied magnetic field. The diamagnetic components due to the substrate and to the $BaTiO_3$ film were subtracted. The data are normalized to the Ni volume considering the mean values of film thickness (17 nm), film porosity (68%), pores diameter (95 nm) and the percentage of pores occupation by Ni nanoparticles (70%). Figures 4a and 4b are consistent with a ferromagnetic behavior of Ni nanoparticles (Curie temperature above room temperature) with a wide size distribution. The maximum magnetization attained at 300 K (Figure 4b) is 300 emu/cm^3, and the coercive fields are around 150 Oe and 25 Oe at 35 K and 300 K, respectively. These values which are lower than the bulk values for Ni (~485 emu/cm^3, and 100 Oe,[39] for saturation magnetization and coercive field, respectively, at 300 K) are attributed to the reduced size of the nanoparticles. Similar values have been reported for Ni nanoparticles.[40] The field variation of the magnetization was also measured at 300 K with the magnetic field perpendicular to the film surface (Figure 4c). In this case, in contrast with the parallel field configuration, a high susceptibility remains up to the highest measured fields, indicating that there is a progressive alignment with the field of the Ni nanoparticles. This result is consistent with the fact that from MFM measurements the domains seem to be oriented parallel to the surface of the film, as an out of plane magnetic contribution was not detected within the pores.

Journal of Materials Chemistry C Accepted Manuscript

View Article Online
DOI: 10.1039/C6TC04232E

Published on 19 December 2016. Downloaded by University of Massachusetts - Amherst on 09/01/2017 14:51:29.

Journal of Materials Chemistry C Accepted Manuscript

Conclusions

Extremely well-patterned composite thin films were fabricated by an easy, chemical-based and scalable method, avoiding costly high-resolution lithography techniques and harmful etching processes. The composites are achieved in two steps encompassing the design of a nanopatterned $BaTiO_3$ porous matrix followed by the filling of the pores with nickel metal nanoparticles using SCFD method. The nanopatterned thin films present a pore diameter size of *ca.* 95 nm and a thickness of *ca.* 17 nm. SEM, EDX and AFM proved the presence of nickel particles with *ca*. 21 nm within the pores. Although through the MFM measurements it was impossible to confirm the magnetic behaviour due to the parallel orientation of the domains, SQUID measurements undoubtedly prove that a magnetic material was successfully deposited in the porous films of $BaTiO_3$.

The amount of the nanoparticles, and subsequent growth can be tuned by controlling the dissolution and reduction time, respectively. The chemical composition of the porous matrix and of the nanoparticles can be modified by the use of different inorganic precursors. This novel strategy of functionalization based in supercritical fluid deposition to create nanocomposite materials is very versatile and can open perspectives for the application of these materials as nanopatterned media (magnetic data storage devices) as well as multiferroic materials.[27–30] A great leap forward in the multiferroic field is expected from alternative and cost effective techniques, easy to be applied to extensive areas, in which the ferroelectric and the ferromagnetic components are arranged with long range ordering and a good control of the stoichiometric composition, phases distribution, interfaces and strain coupling between phases.[30]

Furthermore, nanocomposite thin films with small magnetic nanoparticles with the pores can be also used as a solution to avoid the magnetostatic interactions between

View Article Online
DOI: 10.1039/C6TC04232E

Published on 19 December 2016. Downloaded by University of Massachusetts - Amherst on 09/01/2017 14:51:29.

neighboring magnetic domains in patterned magnetic media by the presence of the walls between the pores.[21,27,41]

Acknowledgements

This work was developed in the scope of the project CICECO-Aveiro Institute of Materials POCI-01-0145-FEDER-007679 (Ref. FCT UID/CTM/50011/2013), financed by national funds through the FCT/MEC and when applicable co-financed by FEDER under the PT2020 Partnership Agreement. Authors are grateful to FCT and POPH/FSE, for doctoral fellowship SFRH/BD/67121/2009 and investigator fellowship IF/00327/2013. This work was also supported by the centre grant BioISI (Ref. UID/MULTI/04046/2013) from FCT/MCTES/PIDDAC, Portugal. A. Cabañas and J. Morère acknowledge the financial support of the Spanish Ministry of Economy and Competitiveness (MINECO), research project CTQ2013-41781. J. Morère thanks MINECO for his support through a predoctoral grant.

References

1 P. Innocenzi, T. Kidchob, P. Falcaro and M. Takahashi, *Chem. Mater.*, 2008, **20**, 607–614.

2 C. Sanchez, C. Boissière, D. Grosso, C. Laberty and L. Nicole, *Chem. Mater.*, 2008, **20**, 682–737.

3 C. Sanchez, C. Boissiere, S. Cassaignon, C. Chaneac, O. Durupthy, M. Faustini, D. Grosso, C. Laberty-Robert, L. Nicole, D. Portehault, F. Ribot, L. Rozes and C. Sassoye, *Chem. Mater.*, 2014, **26**, 221–238.

4 D. Grosso, C. Boissière, B. Smarsly, T. Brezesinski, N. Pinna, P. a Albouy, H. Amenitsch, M. Antonietti and C. Sanchez, *Nat. Mater.*, 2004, **3**, 787–92.

Journal of Materials Chemistry C Accepted Manuscript

View Article Online
DOI: 10.1039/C6TC04232E

Published on 19 December 2016. Downloaded by University of Massachusetts - Amherst on 09/01/2017 14:51:29.

5 P. Ferreira, R. Z. Hou, A. Wu, M.-G. Willinger, P. M. Vilarinho, J. Mosa, C. Laberty-Robert, C. Boissière, D. Grosso and C. Sanchez, *Langmuir*, 2012, **28**, 2944–2949.

6 A. Castro, P. Ferreira, B. J. Rodriguez and P. M. Vilarinho, *J. Mater. Chem. C*, 2015, **3**, 1035–1043.

7 A. Castro, P. Ferreira and P. M. Vilarinho, *J. Phys. Chem. C*, 2016, **120**, 10961–10967.

8 L. W. Martin, S. P. Crane, Y.-H. Chu, M. B. Holcomb, M. Gajek, M. Huijben, C.-H. Yang, N. Balke and R. Ramesh, *J. Phys. Condens. Matter*, 2008, **20**, 434220–13.

9 F. Cansell and C. Aymonier, *J. Supercrit. Fluids*, 2009, **47**, 508–516.

10 E. Reverchon and R. Adami, *J. Supercrit. Fluids*, 2006, **37**, 1–22.

11 J. D. Holmes, D. M. Lyons and K. J. Ziegler, *Chem. Eur. J.*, 2003, **9**, 2145–51.

12 C. Aymonier, A. Loppinet-Serani, H. Reverón, Y. Garrabos and F. Cansell, *J. Supercrit. Fluids*, 2006, **38**, 242–251.

13 M. J. Tenorio, C. Pando, J. A. R. Renuncio, J. G. Stevens, R. A. Bourne, M. Poliakoff and A. Cabañas, *J. Supercrit. Fluids*, 2012, **69**, 21–28.

14 M. Škerget, Z. Knez and M. Knez-Hrnčič, *J. Chem. Eng. Data*, 2011, **56**, 694–719.

15 N. G. Smart, T. Carleson, T. Kast, A. A. Clifford, M. D. Burford and C. M. Wai, *Talanta*, 1997, **44**, 137–150.

16 O. Aschenbrenner, S. Kemper, N. Dahmen, K. Schaber and E. Dinjus, *J. Supercrit. Fluids*, 2007, **41**, 179–186.

17 J. Ming, C. Wu, H. Cheng, Y. Yu and F. Zhao, *J. Supercrit. Fluids*, 2011, **57**, 137–142.

Journal of Materials Chemistry C Accepted Manuscript

View Article Online
DOI: 10.1039/C6TC04232E

Published on 19 December 2016. Downloaded by University of Massachusetts - Amherst on 09/01/2017 14:51:29.

18 J. J. Watkins, J. M. Blackburn and T. J. McCarthy, *Chem. Mater.*, 1999, **11**, 213–215.

19 J. J. Watkins and T. J. McCarthy, *Chem. Mater.*, 1995, **7**, 1991–1994.

20 J. M. Blackburn, D. P. Long, A. Cabanas and J. J. Watkins, *Science*, 2001, **294**, 141–145.

21 E. T. Hunde and J. J. Watkins, *Chem. Mater.*, 2004, **16**, 498–503.

22 S. E. Bozbag, D. Sanli and C. Erkey, *J. Mater. Sci.*, 2011, **47**, 3469–3492.

23 C. Erkey, *J. Supercrit. Fluids*, 2009, **47**, 517–522.

24 S. E. Bozbag, L. C. Zhang, M. Aindow and C. Erkey, *J. Supercrit. Fluids*, 2012, **66**, 265–273.

25 J. Morère, S. Royuela, G. Asensio, P. Palomino, E. Enciso, C. Pando and A. Cabañas, *Philos. Trans. R. Soc. A Math. Phys. Eng. Sci.*, 2015, **373**, 20150014.

26 Q. Peng, J. C. Spagnola and G. N. Parsons, *J. Electrochem. Soc.*, 2008, **155**, D580.

27 C. A. Ross, H. I. Smith and M. Walsh, *J. Vac. Sci. Technol. B*, 1999, **17**, 3168–3176.

28 J. S. Andrew, J. D. Starr and M. A. K. Budi, *Scr. Mater.*, 2014, **74**, 38–43.

29 C. A. F. Vaz, J. Hoffman, C. H. Ahn and R. Ramesh, *Adv. Mater.*, 2010, **22**, 2900–2918.

30 J. F. Scott, *J. Mater. Chem.*, 2012, **22**, 4567.

31 C. A. Schneider, W. S. Rasband and K. W. Eliceiri, *Nat. Methods*, 2012, **9**, 671–675.

32 M. Kuemmel, J. Allouche, L. Nicole, C. Boissière, C. Laberty, H. Amenitsch, C. Sanchez and D. Grosso, *Chem. Mater.*, 2007, **19**, 3717–3725.

33 M. Järn, F. J. Brieler, M. Kuemmel, D. Grosso and M. Lindén, *Chem. Mater.*,

Journal of Materials Chemistry C Accepted Manuscript

View Article Online
DOI: 10.1039/C6TC04232E

2008, **20**, 1476–1483.

34 E. L. Crepaldi, G. J. de A. A. Soler-Illia, D. Grosso, F. Cagnol, F. Ribot and C. Sanchez, *J. Am. Chem. Soc.*, 2003, **125**, 9770–86.

35 D. Grosso, F. Cagnol, G. J. de A. A. Soler-Illia, E. L. Crepaldi, H. Amenitsch, A. Brunet-Bruneau, A. Bourgeois and C. Sanchez, *Adv. Funct. Mater.*, 2004, 14, 309–322.

36 C. Dubourdieu, J. Bruley, T. M. Arruda, A. Posadas, J. Jordan-Sweet, M. M. Frank, E. Cartier, D. J. Frank, S. V Kalinin, A. A. Demkov and V. Narayanan, *Nat. Nanotechnol.*, 2013, **8**, 748–54.

37 L. Suresh and J. Y. Walz, *J. Colloid Interface Sci.*, 1996, **183**, 199–213.

38 E. Kondoh, *Japanese J. Appl. Physics, Part 1 Regul. Pap. Short Notes Rev. Pap.*, 2005, **44**, 5799–5802.

39 B. D. Cullity and C. D. Graham, *Introduction to Magnetic Materials*, Hoboken, New Jersey, 2nd edn., 2009.

40 X. He, W. Zhong, C.-T. Au and Y. Du, *Nanoscale Res. Lett.*, 2013, **8**, 446.

41 C. Ross, *Annu. Rev. Mater. Res.*, 2001, **31**, 203–235.

Published on 19 December 2016. Downloaded by University of Massachusetts - Amherst on 09/01/2017 14:51:29.

Journal of Materials Chemistry C Accepted Manuscript

View Article Online
DOI: 10.1039/C6TC04232E

Published on 19 December 2016. Downloaded by University of Massachusetts - Amherst on 09/01/2017 14:51:29.

Figure Captions

Figure 1. SEM of nanopatterned $BaTiO_3$ thin films before (a-c) and after (e-f) functionalization with Ni nanoparticles through SCFD. The insets present in the Figures a-c show a zoom of the respective SEM micrographs showing the well-ordered porous structure. The pore size is around 95 nm and the Ni nanoparticles size is less that 21 nm. EDX patterns of the nanopatterned thin films after functionalization with Ni nanoparticles is represented in g). In d) is schematically illustrated the approach used to functionalize the nanopatterned thin films with Ni nanoparticles.

Figure 2. AFM topography images (1μm x 1 μm) of nanopatterned BaTiO3 thin films: a) before and b) after functionalization with Ni nanoparticles through SCFD. The images show a well-ordered porous array and the nanoparticles are only within the pores. No big particles can be observed.

Figure 3. a) Topography AFM (750 nm x 750 nm) and b) MFM phase images of nanopatterned $BaTiO_3$ thin films deposited after functionalization with Ni by SCFD. The nanocomposite thin films do not present any contrast even at 5 nm from the surface suggesting the parallel orientation of the domains in relation to the surface. The slight contrast observed is a topographic effect due to the small distance between the tip and surface.

Figure 4. Magnetization normalized to the volume of Ni nanoparticles estimated from SEM and AFM measurements, after subtraction of the diamagnetic components: a) ZFC-FC curves measured under an applied field of 200 Oe; b) Hysteresis loops obtained at 35 and 300 K in parallel configuration; c) Hysteresis curves obtained at 300 K, with the magnetic field applied parallel and perpendicular to the film surface.

Journal of Materials Chemistry C Accepted Manuscript

View Article Online
DOI: 10.1039/C6TC04232E

Published on 19 December 2016. Downloaded by University of Massachusetts - Amherst on 09/01/2017 14:51:29.

Figures

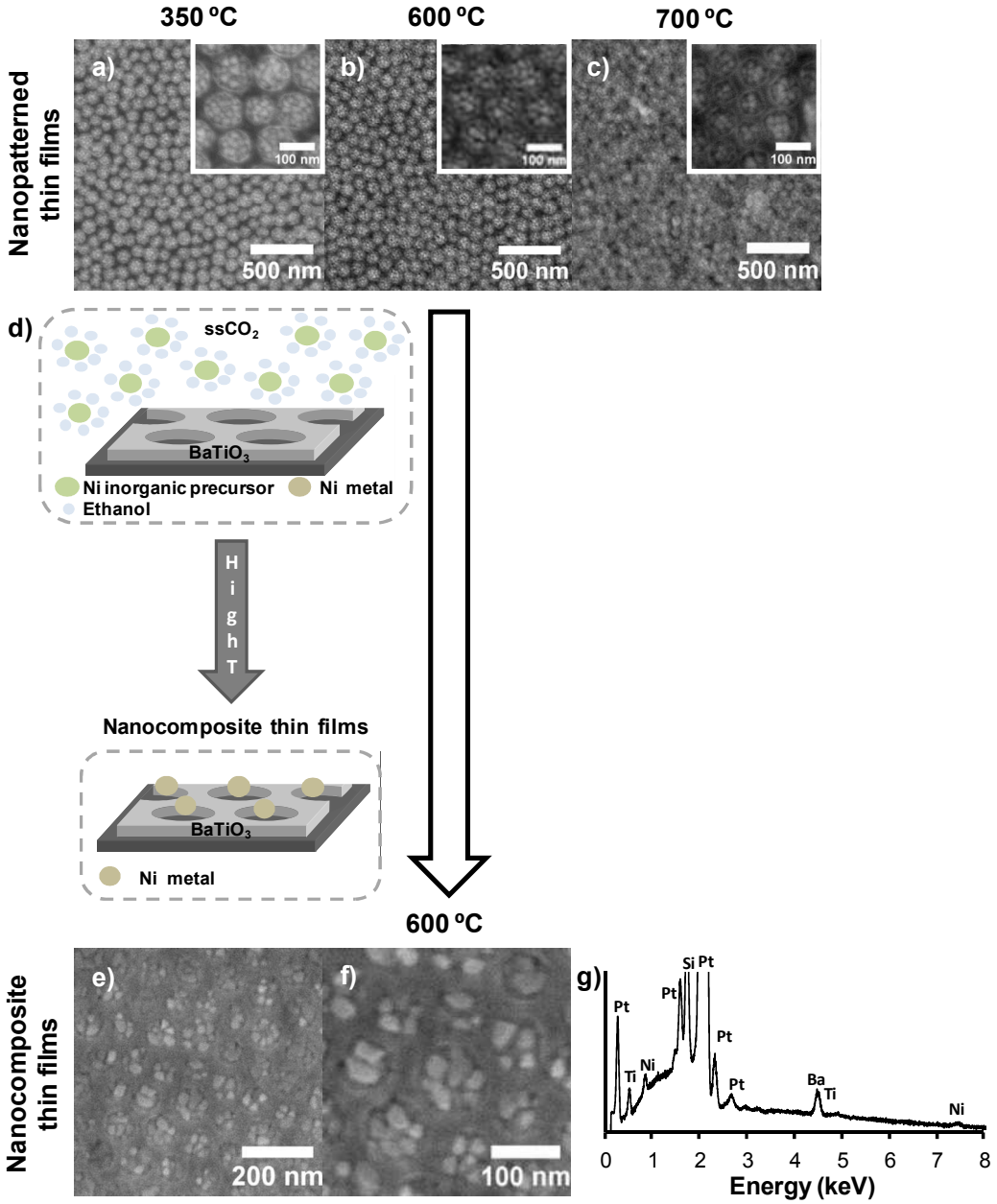

Figure 1. SEM of nanopatterned $BaTiO_3$ thin films before (a-c) and after (e-f) functionalization with Ni nanoparticles through SCFD. The insets present in the Figures a-c show a zoom of the respective SEM micrographs showing the well-ordered porous structure. The pore size is around 95 nm and the Ni nanoparticles size is around 21 nm. EDX patterns of the nanopatterned thin films after functionalization with Ni nanoparticles is represented in g). In d) is schematically illustrated the approach used to functionalize the nanopatterned thin films with Ni nanoparticles.

Journal of Materials Chemistry C Accepted Manuscript

View Article Online
DOI: 10.1039/C6TC04232E

Published on 19 December 2016. Downloaded by University of Massachusetts - Amherst on 09/01/2017 14:51:29.

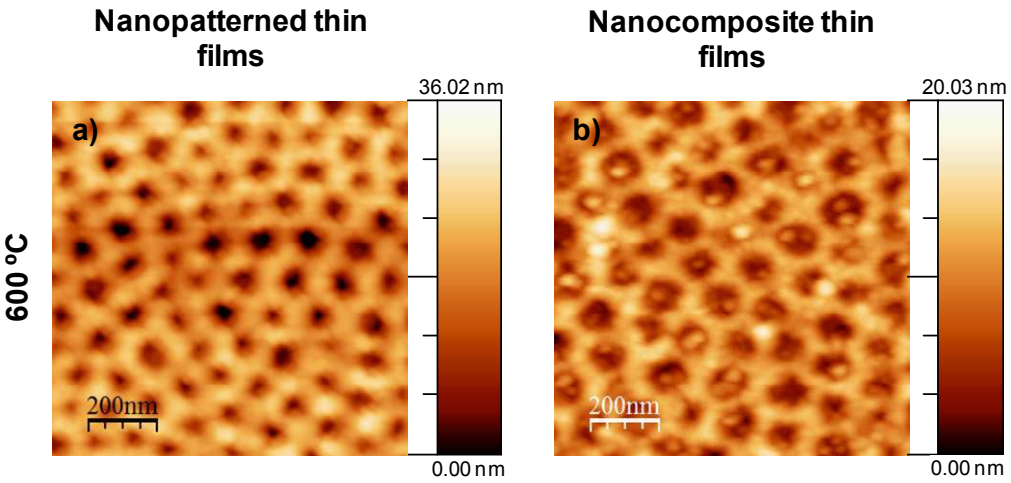

Figure 2. AFM topography images (1µm x 1 µm) of nanopatterned $BaTiO_3$ thin films: a) before and b) after functionalization with Ni nanoparticles through SCFD. The images show a well-ordered porous array and the nanoparticles are only within the pores. No big particles can be observed.

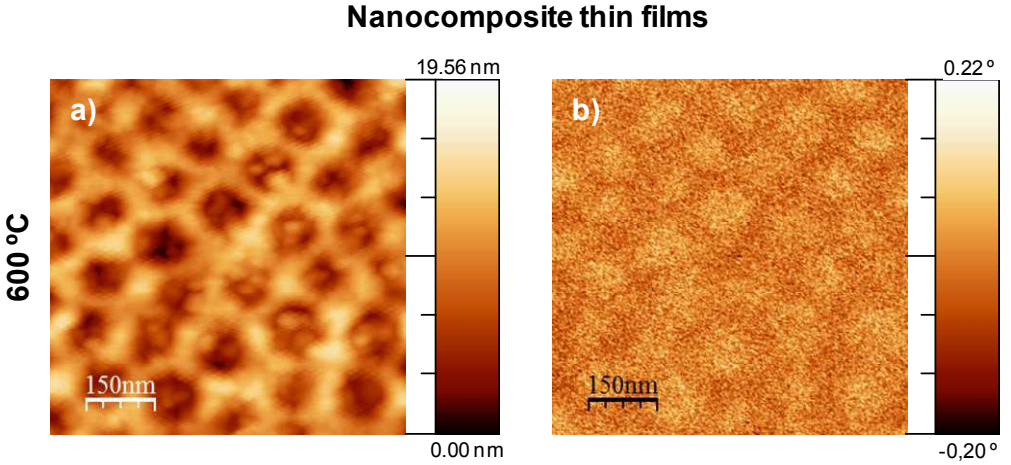

Figure 3. a) Topography AFM (750 nm x 750 nm) and b) MFM phase images of nanopatterned $BaTiO_3$ thin films deposited after functionalization with Ni by SCFD. The nanocomposite thin films do not present any contrast even at 5 nm from the surface suggesting the parallel orientation of the domains in relation to the surface. The slight contrast observed is a topographic effect due to the small distance between the tip and surface.

Journal of Materials Chemistry C Accepted Manuscript

View Article Online
DOI: 10.1039/C6TC04232E

Published on 19 December 2016. Downloaded by University of Massachusetts - Amherst on 09/01/2017 14:51:29.

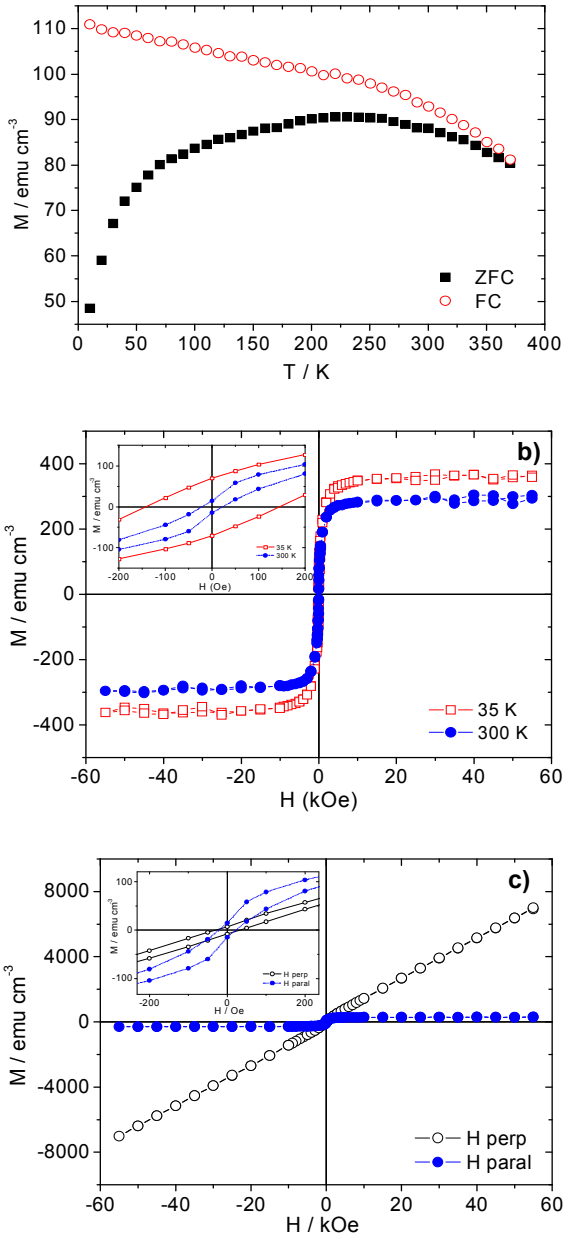

Figure 4. Magnetization normalized to the volume of Ni nanoparticles estimated from SEM and AFM measurements, after subtraction of the diamagnetic components: a) ZFC-FC curves measured under an applied field of 200 Oe; b) Hysteresis loops obtained at 35 and 300 K in parallel configuration; c) Hysteresis curves obtained at 300 K, with the magnetic field applied parallel and perpendicular to the film surface.

Journal of Materials Chemistry C Accepted Manuscript

View Article Online
DOI: 10.1039/C6TC04232E

Published on 19 December 2016. Downloaded by University of Massachusetts - Amherst on 09/01/2017 14:51:29.

Table of Contents (TOC)

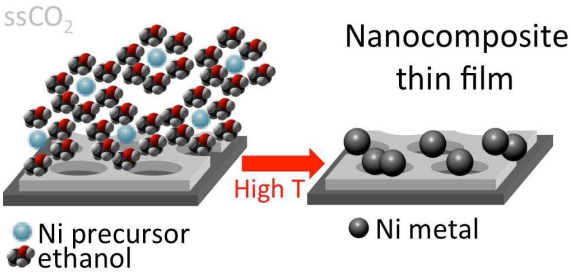

Supercritical CO_2 deposition: a tool to achieve multifunctional materials starting from a porous platform.

Journal of Materials Chemistry C Accepted Manuscript